

A mathematical model and inversion procedure for Magneto-Acousto-Electric Tomography (MAET)

Leonid Kunyansky

February 17, 2022

Abstract

Magneto-Acousto-Electric Tomography (MAET), also known as the Lorentz force or Hall effect tomography, is a novel hybrid modality designed to be a high-resolution alternative to the unstable Electrical Impedance Tomography. In the present paper we analyze existing mathematical models of this method, and propose a general procedure for solving the inverse problem associated with MAET. It consists in applying to the data one of the algorithms of Thermo-Acoustic tomography, followed by solving the Neumann problem for the Laplace equation and the Poisson equation.

For the particular case when the region of interest is a cube, we present an explicit series solution resulting in a fast reconstruction algorithm. As we show, both analytically and numerically, MAET is a stable technique yielding high-resolution images even in the presence of significant noise in the data.

Introduction

Magneto-Acousto-Electric Tomography (MAET) is based on the measurements of the electrical potential arising when an acoustic wave propagates through conductive medium placed in a constant magnetic field [26, 34]. The interaction of the mechanical motion of the free charges (ions and/or electrons) with the magnetic field results in the Lorentz force that pushes charges of different signs in opposite directions, thus generating Lorentz currents within the tissue. The goal of this technique coincides with that of the Electrical Impedance Tomography (EIT): to reconstruct the conductivity of the tissue from the values of the electric potential measured on the boundary of the object. EIT is a fast, inexpensive, and harmless modality, which is potentially very valuable due to the large contrast in the conductivity between healthy and cancerous tissues [5, 6, 9]. Unfortunately, the reconstruction problems arising in EIT are known to be exponentially unstable.

MAET is one of the several recently introduced hybrid imaging techniques designed to stabilize the reconstruction of electrical properties of the tissues by coupling together ultrasound waves with other physical phenomena. Perhaps the best known examples of hybrid methods are the Thermo-Acoustic Tomography (TAT) [16] and the closely related Photo-Acoustic modality, PAT [15, 29]). In the latter methods the amount of electromagnetic energy absorbed by the medium is reconstructed from the measurements (on the surface

of the object) of acoustic waves caused by the thermoacoustic expansion (see e.g. [17, 33]). Another hybrid technique, designed to overcome shortcomings of EIT and yield stable reconstruction of the conductivity is Acousto-Electric Impedance Tomography (AEIT) [36]. It couples together acoustic waves and electrical currents, through the electroacoustic effect (see [25]). Although AEIT has been shown, both theoretically and in numerical simulations, to be stable and capable of yielding high-resolution images [3, 8, 18, 19], the feasibility of practical reconstructions is still in question due to the extreme weakness of the acousto-electric effect.

In the present paper we analyze MAET which also aims to reconstruct the conductivity in a stable fashion. In MAET this goal is achieved by combining magnetic field, acoustic excitation and electric measurements, coupled through the Lorentz force. The physical foundations of MAET were established in [26] and [34]. In particular, it was shown in [26] that if the tissue with conductivity $\sigma(x)$ moves with velocity $V(x, t)$ within the constant magnetic field B , the arising Lorentz force will generate Lorentz currents $J_L(x, t)$ whose intensity and direction are given (approximately) by the following formula

$$J_L(x, t) = \sigma(x)B \times V(x, t). \quad (1)$$

Originally [26, 34] it was proposed to utilize a focused propagating acoustic pulse to induce electric response from different parts of the object. In [13] wavepackets of a certain frequency were used in a physical experiment to reconstruct the current density in a thin slab of a tissue. Similarly, in [4] the use of a perfectly focused acoustic beam was assumed in a theoretical study and in numerical simulations. However, in the above-quoted works accurate mathematical model(s) of such beams were not presented. Moreover, the feasibility of focusing a fixed frequency acoustic beam at an arbitrary point inside the body in a fully 3D problem is problematic. In a theoretical study [30] the use of plane waves of varying frequencies was proposed instead of the beams. This is a more realistic approach; however, the analysis in that work relies on several crude approximations (the conductivity is assumed to be close to 1, and the electric field is approximated by the first non-zero term in the multipole expansion).

To summarize, the existing mathematical models of measurements in MAET are of approximate nature; moreover, some of them contradict to others. For example, it was found in [13] that if one uses a pair of electrodes to measure the voltage (difference of the potentials) at two points a and b on the boundary of the body, the result is the integral of the mixed product of three vectors: velocity V , magnetic induction B and the so-called lead current J_{ab} (the current that would flow in the body if the difference of potentials were applied at points a and b). The approximate model in [30] implicitly agrees with this conclusion. However, in [4] it is assumed that if the pulse is focused at the point x , the measurements will be proportional to the product of the electric potential $u(x)$ and conductivity $\sigma(x)$ at that point. This assumption contradicts the previous models; it also seems to be unrealistic since potential $u(x)$ is only defined up to an arbitrary constant, while the measurements are completely determined by the physics of the problem.

In the present paper we first derive, starting from equation (1), a rigorous and sufficiently general model of the MAET measurements. Next, we show that if a sufficient amount of data is measured, one can reconstruct, almost explicitly and in a stable fashion the conductivity of the tissue. For general domains the reconstruction can be reduced to the solution of the

inverse problem of TAT followed by the solution of the Neumann problem for the Laplace equation, and a Poisson equation. In the simpler case of a rectangular domain the reconstruction formulae can be made completely explicit, and the solution is obtained by summing several Fourier series. In the latter case the algorithm is fast, i.e. it runs in $O(n^3 \log n)$ floating point operations on a $n \times n \times n$ grid. The results of our numerical simulations show that one can stably recover high resolution images of the conductivity of the tissues from MAET measurements even in the presence of a significant noise in the data.

1 Formulation of the problem

Suppose that the object of interest whose conductivity $\sigma(x)$ we would like to recover is supported within an open and bounded region Ω with the boundary $\partial\Omega$. For simplicity we will assume that $\sigma(x)$ is smooth in Ω , does not approach 0, and equals 1 in the vicinity of $\partial\Omega$; the support of $\sigma(x) - 1$ lies in some $\Omega_1 \subset \Omega$ and the distance between Ω_1 and $\partial\Omega$ is non-zero. The object is placed in the magnetic field with a constant magnetic induction B , and an acoustic wave generated by a source lying outside Ω propagates through the object with the velocity $V(x, t)$. Then the Lorentz force will induce Lorentz currents in Ω given by equation (1). Throughout the text we assume that the electrical interactions occur on much faster time scale than the mechanical ones, and so all currents and electric potentials depend on t only as a parameter. In addition to Lorentz currents, the arising electrical potential $u(x, t)$ will generate secondary, Ohmic currents with intensities given by Ohm's law

$$J_O(x, t) = \sigma(x) \nabla u(x, t).$$

Since there are no sinks or sources of electric charges within the tissues, the total current $J_L(x, t) + J_O(x, t)$ is divergence-free

$$\nabla \cdot (J_L + J_O) = 0.$$

Thus

$$\nabla \cdot \sigma \nabla u = -\nabla \cdot (\sigma B \times V). \quad (2)$$

Since there are no currents through the boundary, the normal component of the total current $J_L(x, t) + J_O(x, t)$ vanishes:

$$\frac{\partial}{\partial n} u(z) = -(B \times V(z)) \cdot n(z), \quad z \in \partial\Omega, \quad (3)$$

where $n(z)$ is the exterior normal to $\partial\Omega$ at point z .

We will assume that the boundary values of the potential $u(z, t)$ can be measured at all points z lying on $\partial\Omega$. More precisely, we will model the measurements by integrating the boundary values with a weight $I(z)$ and thus forming measuring functional M defined by the formula

$$M(t) = \int_{\partial\Omega} I(z) u(z, t) dA(z), \quad (4)$$

where $A(z)$ is the standard area element. Weight $I(z)$ can be a function or a distribution, subject to the restriction

$$\int_{\partial\Omega} I(z) dA(z) = 0.$$

In particular, if one chooses to use $I(z) = \delta(z - a) - \delta(z - b)$, where $\delta(\cdot)$ is the 2D Dirac delta-function, then M models the two-point measuring scheme utilized in [13] and [30].

In order to understand what kind of information is encoded in the values of $M(t)$ let us consider solution $w_I(x)$ of the following divergence equation

$$\nabla \cdot \sigma \nabla w_I(x) = 0, \quad (5)$$

$$\frac{\partial}{\partial n} w_I(z) = I(z), \quad z \in \partial\Omega. \quad (6)$$

(To ensure the uniqueness of the solution of the above boundary value problem we will require that the integral of $w_I(z)$ over Ω vanishes.) Then $w_I(x)$ equals the electric potential that would be induced in the tissues by injecting currents $I(z)$ at the boundary $\partial\Omega$. Let us denote the corresponding currents $\sigma \nabla w_I(x)$ by $J_I(x)$:

$$J_I(x) = \sigma \nabla w_I(x). \quad (7)$$

Let us now apply the second Green's identity to functions $u(x, t)$, $w_I(x)$, and $\sigma(x)$:

$$\int_{\Omega} [w_J \nabla \cdot (\sigma \nabla u) - u \nabla \cdot (\sigma \nabla w_J)] dx = \int_{\partial\Omega} \sigma \left[w_J \frac{\partial}{\partial n} u - u \frac{\partial}{\partial n} w_J \right] dA(z). \quad (8)$$

By taking into account (3), (2), (5), and (6), equation (8) can be simplified to

$$- \int_{\Omega} w_J \nabla \cdot (\sigma B \times V) dx = \int_{\partial\Omega} \sigma w_J \frac{\partial}{\partial n} u dA(z) - M(t).$$

Further, by integrating the left hand side of the last equation by parts, and by replacing $\frac{\partial}{\partial n} u$ with expression (3) we obtain

$$\int_{\Omega} \sigma \nabla w_J \cdot (B \times V) dx - \int_{\partial\Omega} w_J \sigma (B \times V) \cdot n dA(z) = - \int_{\partial\Omega} \sigma w_J (B \times V) \cdot n dA(z) + M(t)$$

or

$$M(t) = - \int_{\Omega} \sigma \nabla w_J \cdot (B \times V) dx = - \int_{\Omega} J_I \cdot (B \times V) dx = B \cdot \int_{\Omega} J_I(x) \times V(x, t) dx \quad (9)$$

This equation generalizes equation (1) in [13] obtained for the particular case $I(z) = \delta(z - a) - \delta(z - b)$.

It is clear from equation (9) that MAET measurements recover some information about currents $J_I(x)$. In order to gain further insight let us assume that the acoustical properties of the medium, such as speed of sound c and density ρ , are approximately constant within

Ω . (Such approximation usually holds in breast imaging which is one of the most important potential applications of this and similar modalities). Then the acoustic pressure $p(x, t)$ within Ω satisfies the wave equation

$$\frac{1}{c^2} \frac{\partial^2}{\partial t^2} p(x, t) = \Delta p(x, t).$$

Additionally, $p(x, t)$ is the time derivative of the velocity potential $\varphi(x, t)$ (see, for example [10]), so that

$$\begin{aligned} V(x, t) &= \frac{1}{\rho} \nabla \varphi(x, t), \\ p(x, t) &= \frac{\partial}{\partial t} \varphi(x, t). \end{aligned} \tag{10}$$

Velocity potential $\varphi(x, t)$ also satisfies the wave equation

$$\frac{1}{c^2} \frac{\partial^2}{\partial t^2} \varphi(x, t) = \Delta \varphi(x, t).$$

Now, by taking into account (10), equation (9) can be re-written as

$$M(t) = \frac{1}{\rho} B \cdot \int_{\Omega} J_I(x) \times \nabla \varphi(x, t) dx$$

Further, by noticing that

$$\nabla \times (\varphi J_I) = -J_I \times \nabla \varphi + \varphi \nabla \times J_I$$

we obtain

$$\begin{aligned} M(t) &= \frac{1}{\rho} B \cdot \left[- \int_{\Omega} \nabla \times (\varphi J_I) dx + \int_{\Omega} \varphi(x, t) \nabla \times J_I(x) dx \right] \\ &= \frac{1}{\rho} B \cdot \left[\int_{\partial\Omega} \varphi(z, t) J_I(z) \times n(z) dA(z) + \int_{\Omega} \varphi(x, t) \nabla \times J_I(x) dx \right]. \end{aligned} \tag{11}$$

In some situations the above equations can be further simplified. For example, if at some moment of time t velocity potential $\varphi(x, t)$ vanishes on the boundary $\partial\Omega$, then the surface integral in (11) also vanishes:

$$M(t) = \frac{1}{\rho} B \cdot \int_{\Omega} \varphi(x, t) \nabla \times J_I(x) dx. \tag{12}$$

Similarly, if boundary $\partial\Omega$ is located far away from the support of inhomogeneity of $\sigma(x)$, the surface integral in (11) can be neglected, and we again obtain equation (12).

Equation (11) is our mathematical model of the MAET measurements. Our goal is to reconstruct from measurements $M(t)$ conductivity $\sigma(x)$ — by varying, if necessary, B , $\varphi(x, t)$, and $I(z)$.

Our strategy for solving this problem is outlined in the following sections. However, some conclusions can be reached just by looking at the equation (11). For example, one can notice that if three sets of measurements are conducted with magnetic induction pointing respectively in the directions of canonical basis vectors e_1 , e_2 , and e_3 , one can easily reconstruct the sum of integrals in the brackets in (11). Further, if one focuses $\varphi(x, t)$ so that at the moment $t = 0$ it becomes the Dirac δ -function centered at y , i.e.

$$\varphi(x, 0) = \delta(x - y)$$

then one immediately obtains the value of $\nabla \times J_I$ at the point y (such a focusing is theoretically possible as explained in the next section). Thus, by moving the focusing point through the object, one can reconstruct the curl of J_I in all of Ω .

Our model also explains the observation reported in [13] that no signal is obtained when the acoustic wavepacket is passing through the regions of the constant $\sigma(x)$. In such regions current J_I is a potential vector field and, therefore, the integral in (12) vanishes.

Finally, it becomes clear that an accurate image reconstruction is impossible if monochromatic acoustic waves of only a single frequency k are used for scanning, no matter how well they are focused. In this case the spatial component ψ of $\varphi(x, t) = \psi(x) \exp(ikt)$ is a solution of the Helmholtz equation

$$\Delta\psi + k^2\psi = 0,$$

and, within Ω it can be approximated by the plane waves in the form $\exp(i\lambda \cdot x)$ with $|\lambda| = k$. Let us assume for simplicity that the electrical boundary is removed to infinity. Then, measuring $M(t)$ given by equation (12) is equivalent to collecting values of the Fourier transform of $\nabla \times J_I(x)$ corresponding to the wave vectors λ lying on the surface of the sphere $|\lambda| = k$ in the Fourier domain. The spatial frequencies of function $\nabla \times J_I(x)$ with wave vectors that do not lie on this sphere cannot be recovered.

2 Solving the inverse problem of MAET

The first step toward the reconstruction of the conductivity is to reconstruct currents $J_I(x)$ corresponding to certain choices of $I(z)$. Let us assume that all the measurements are repeated three times, with magnetic induction B pointing respectively in the directions of canonical basis vectors e_1 , e_2 , and e_3 . Then, as mentioned above, if $\varphi(x, 0) = \delta(x - y)$, one readily recovers from the measurements $M(0)$ the curl of the current at y , i.e. $\nabla \times J_I(y)$. Generating such a velocity potential is possible at least theoretically. For example, if one simultaneously propagates plane waves $\varphi_\lambda(x, t) = \exp(i\lambda \cdot x - i|\lambda|t)$ with all possible wave vectors λ , the combined velocity potential at the moment $t = 0$ will add up to the Dirac delta-function $\delta(x)$. Such an arrangement is unlikely to be suitable for a practical implementation: firstly, the sources of sound would have to be removed far from the object to produce a good approximation to plane waves within the object. Secondly, the sources would have to completely surround the object to irradiate it from all possible directions. Finally, all the sources would have to be synchronized. A variation of this approach is to place small

point-like sources in the vicinity of the object. In this case, instead of plane waves, spherical monochromatic waves or propagating spherical fronts would be generated. These types of waves can also be focused into a delta-function (some discussion of such focusing and a numerical example can be found in [19]).

2.1 Synthetic focusing

However, a more practical approach is to utilize some realistic measuring configuration (e.g. one consisting of one or several small sources scanning the boundary sequentially), and then to synthesize algorithmically from the realistic data the desired measurements that correspond to the delta-like velocity potential. Such a *synthetic focusing* was first introduced in the context of hybrid methods in [18, 19, 24]. It was shown, in applications to AET and to the acoustically modulated optical tomography, that such a synthetic focusing is equivalent to solving the inverse problem of TAT. The latter problem has been studied extensively, and a wide variety of methods is known by now (we will refer the reader to reviews [17, 33] and references therein). The same technique can be applied to MAET, as explained below.

2.1.1 Measuring functionals solve the wave equation

Let us consider a spherical propagating front originated at the point y . If the initial conditions on the pressure $p_y(x, t)$ are

$$\begin{cases} p_y(x, 0) = \delta(x - y), \\ \frac{\partial}{\partial t} p_y(x, 0) = 0, \end{cases}$$

then $p_y(x, t)$ can be represented in the whole of \mathbb{R}^3 by means of the Kirchhoff formula [32]

$$p_y(x, t) = \frac{\partial}{\partial t} \frac{\delta(|x - y| - ct)}{4\pi|x - y|}.$$

Such a front can be generated by a small transducer placed at y and excited by a delta-like electric pulse; such devices are common in ultrasonic imaging.

Velocity potential $\varphi(x, y, t)$ corresponding to $p_y(x, t)$ then equals

$$\varphi(x, y, t) = \frac{\delta(|x - y| - ct)}{4\pi|x - y|}. \quad (13)$$

The role of variables x and y is clearly interchangeable; $\varphi(x, y, t)$ is the retarded Green's function of the wave equation [32] either in x and t , or in y and t . Moreover, consider the following convolution $H(y, t)$ of a finitely supported smooth function $h(y)$ with φ

$$H(y, t) = \int_{\mathbb{R}^3} h(y) \frac{\delta(|x - y| - ct)}{4\pi|x - y|} dx.$$

Then $H(y, t)$ is the solution of the following initial value problem (IVP) in \mathbb{R}^3 [32]:

$$\begin{cases} \frac{1}{c^2} \frac{\partial^2}{\partial t^2} H(y, t) = \Delta_y H(y, t) \\ H(y, 0) = 0, \\ \frac{\partial}{\partial t} H(y, 0) = h(y). \end{cases} \quad (14)$$

Suppose now that a set of MAET measurements is obtained with propagating wave fronts $\varphi(x, y, t)$ with different centers y (while $I(z)$ and B are kept fixed). By substituting (13) into (11) we find that, for each y , the corresponding measuring functional $M_{I,B}(y, t)$ can be represented as the sum of two terms:

$$M_{I,B}(y, t) = M_{I,B}^{\text{sing}}(y, t) + M_{I,B}^{\text{reg}}(y, t),$$

where

$$M_{I,B}^{\text{sing}}(y, t) = \frac{1}{\rho} \int_{\partial\Omega} \frac{\delta(|z - y| - ct)}{4\pi|z - y|} B \cdot J_I(z) \times n(z) dA(z), \quad (15)$$

$$M_{I,B}^{\text{reg}}(y, t) = \frac{1}{\rho} \int_{\Omega} \frac{\delta(|x - y| - ct)}{4\pi|x - y|} B \cdot \nabla \times J_I(x) dx. \quad (16)$$

It is clear from the above discussion that both terms $M_{I,B}^{\text{sing}}(y, t)$ and $M_{I,B}^{\text{reg}}(y, t)$ solve the wave equation in \mathbb{R}^3 , subject to the initial conditions

$$\frac{\partial}{\partial t} M_{I,B}^{\text{sing}}(x, 0) = \frac{1}{\rho} B \cdot J_I(x) \times n(x) \delta_{\partial\Omega}(x), \quad (17)$$

$$\frac{\partial}{\partial t} M_{I,B}^{\text{reg}}(x, 0) = \frac{1}{\rho} B \cdot \nabla \times J_I(x), \quad (18)$$

$$M_{I,B}^{\text{sing}}(y, t) = M_{I,B}^{\text{reg}}(y, t) = 0, \quad (19)$$

where $\delta_{\partial\Omega}(x)$ is the delta-function supported on $\partial\Omega$. While singular term $M_{I,B}^{\text{sing}}(y, t)$ solves the wave equation in the sense of distributions, the regular term $M_{I,B}^{\text{reg}}(y, t)$ represents a classical solution of the wave equation.

Proposition 1 *Suppose conductivity $\sigma(x)$ and boundary currents $I(z)$ are C^∞ functions of their arguments, and the boundary $\partial\Omega$ is infinitely smooth. Then the regular part $M_{I,B}^{\text{reg}}(y, t)$ of the measuring functional is a C^∞ solution of the wave equation*

$$\frac{1}{c^2} \frac{\partial^2}{\partial t^2} M_{I,B}^{\text{reg}}(y, t) = \Delta_y M_{I,B}^{\text{reg}}(y, t), \quad y \in \mathbb{R}^3, \quad t \in [0, \infty), \quad (20)$$

satisfying initial conditions (18) and (19).

Proof. Under the above conditions, potential $w_I(x)$ solving the boundary value problem (5), (6) is a C^∞ function in Ω due to the classical estimates on the smoothness of solutions of elliptic equations with smooth coefficients [12]. Therefore, the right hand side of (18) can be extended by zero to a C^∞ function in \mathbb{R}^3 . Term $M_{I,B}^{\text{reg}}(y, t)$ defined by equation (16) solves wave equation (20) (due to the Kirchhoff formula, see [32]) subject to infinitely smooth initial conditions (18), (19), and thus it is a C^∞ function for all $y \in \mathbb{R}^3$, $t \in [0, \infty)$. ■

2.1.2 Reconstructing the initial conditions

We would like to reconstruct the right hand side of (18) (and, possibly that of (17)) from the measured values of $M_{I,B}(y, t)$. Since c is assumed constant, in the 3D case $M_{I,B}(y, t)$ will vanish (due to the Huygens principle) for $t > t_{\max} = D_{\max}/c$ where D_{\max} is the maximal distance between the points of Ω and the acoustic sources. We will assume that $M_{I,B}(y, t)$ is measured for all $t \in [0, t_{\max}]$.

The problem of reconstructing $\frac{\partial}{\partial t} M_{I,B}(x, 0)$ from $M_{I,B}(y, t)$ is equivalent to that of reconstructing the initial value $h(y)$ from the solution of IVP (14). The latter, more general problem, has been studied extensively in the context of TAT (see, e.g. [17, 33] and references therein). In the case of TAT, points y describe the location of detectors rather than sources, but the rest of the mathematics remains the same. The most studied situation is when the detectors are placed on a closed surface Σ surrounding the object. If Σ is a sphere, a variety of inversion techniques is known, including (but not limited to) the explicit inversion formulae [11, 20, 28], series techniques [21, 23, 27, 35], time reversal by means of finite differences [2, 7, 14], etc. If Σ is a surface of a cube, one can use the inversion formula [22], the already mentioned time reversal methods, or the fast algorithm developed in [21] for such surfaces.

The choice of the TAT inversion method for application in MAET will depend, in particular, on the mutual location of the electric boundary $\partial\Omega$ and the acoustic source surface Σ . One can decide to move the electric boundary further away by placing the object in a liquid with conductivity equal to 1 and by submerging the acoustic sources into the liquid, in which case Σ will be inside $\partial\Omega$. Alternatively, one can move the acoustic surface further away so that it surrounds the electric boundary. And, finally, one may choose to conduct the electrical measurements on the surface of the body, and to place the acoustic sources on the same surface, in which case Σ will coincide with $\partial\Omega$.

If $\partial\Omega$ lies inside Σ , all the above mentioned TAT inversion techniques (theoretically) will reconstruct both $M_{I,B}^{\text{sing}}(y, 0)$ and $M_{I,B}^{\text{reg}}(y, 0)$. In practice, accurate numerical reconstruction of the singular term $M_{I,B}^{\text{sing}}(y, 0)$ supported on $\partial\Omega$ may be difficult to obtain due to the finite resolution of any realistic measurement system. Luckily, the support of $M_{I,B}^{\text{reg}}(y, 0)$ (Ω_1 in our notation) is spatially separated from $\partial\Omega$, so that the contributions from the singular term can be eliminated just by setting the reconstructed image to zero outside Ω_1 . As explained further in the paper, $M_{I,B}^{\text{reg}}(y, 0)$ contains enough information to reconstruct the conductivity. On the other hand, $M_{I,B}^{\text{sing}}(y, 0)$ does carry some useful information, which can be recovered by a specialized reconstruction algorithm.

If Σ lies inside $\partial\Omega$ (but Ω_1 still lies inside Σ), not all TAT reconstruction techniques can be applied. Most inversion formulae will produce an incorrect result in the presence of the exterior sources (such as the term $M_{I,B}^{\text{sing}}(y, 0)$ supported on $\partial\Omega$ and exterior with respect to the region enclosed by Σ). On the other hand, formula [22], series methods [21] and all the time reversal techniques automatically filter out the exterior sources and thus can be used to reconstruct $M_{I,B}^{\text{reg}}(y, 0)$.

The situation is more complicated if surfaces Σ and $\partial\Omega$ coincide. However, those methods that are insensitive to sources located outside $\partial\Omega$ are also insensitive to the sources located on $\partial\Omega$, particularly to those represented by $M_{I,B}^{\text{sing}}(y, 0)$. These methods can be used to reconstruct $M_{I,B}^{\text{reg}}(y, 0)$. In other words, the following proposition holds:

Proposition 2 *If values of measuring functional $M_{I,B}(y, t)$ are known for all $y \in \Sigma$ and $t \in [0, D_{\max}/c]$, the term $M_{I,B}^{\text{reg}}(y, 0)$ can be exactly reconstructed in Ω_1 (by using one of the above-mentioned TAT algorithms). Moreover, if the conditions of Proposition 1 are satisfied, the reconstruction is exact point-wise.*

Reconstructing the curl In order to reconstruct the curl of the current $J_I(x)$, we need to repeat the procedure of finding $M_{I,B}^{\text{reg}}(x, 0)$ times, with three different orientations of B : $B^{(j)} = |B|e_j$, $j = 1, 2, 3$. As a result, we find the projections of $\nabla \times J_I(x)$ curl on e_1, e_2, e_3 and thus obtain:

$$\nabla \times J_I(x) = \frac{\rho}{|B|} \sum_{j=1}^3 e_j \frac{\partial}{\partial t} M_{I,B^{(j)}}^{\text{reg}}(x, 0), \quad x \in \Omega_1. \quad (21)$$

(outside Ω_1 the curl of $J_I(x)$ equals 0 since the conductivity is constant there).

If, in addition, $\partial\Omega$ lies inside Σ and $M_{I,B}^{\text{sing}}(y, 0)$ has been reconstructed, we obtain the term

$$J_I(x) \times n(x) \delta_{\partial\Omega}(x) = \frac{\rho}{|B|} \sum_{j=1}^3 e_j \frac{\partial}{\partial t} M_{I,B^{(j)}}^{\text{sing}}(x, 0). \quad (22)$$

2.2 Reconstructing the currents

The considerations of the previous section show how to recover from the values of the measuring functionals $M_{I,B^{(j)}}(y, t)$ the curl of the current J_I and, in some situations, the surface term (22). The next step is to reconstruct current J_I itself.

2.2.1 General situation

Let us start with the most general situation and assume that only the curl $C = \nabla \times J_I$ has been reconstructed. Since current J_I is a purely solenoidal field, there exists a vector potential $K(x)$ such that

$$J_I(x) = \nabla \times K(x) + \Psi(x), \quad (23)$$

where $K(x)$ has the form

$$K(x) = \int_{\Omega} \frac{C(y)}{4\pi(x-y)} dy,$$

and $\Psi(x)$ is both a solenoidal and potential field. Then there exists harmonic $\psi(x)$ such that

$$\Psi(x) = \nabla \psi(x). \quad (24)$$

We know that

$$J_I \cdot n|_{\partial\Omega} = \frac{\partial}{\partial n} w_I \Big|_{\partial\Omega} = I. \quad (25)$$

Therefore, by combining equations (23) and (25) one obtains

$$\left(n \cdot (\nabla \times K)(z) + \frac{\partial}{\partial n} \psi(z) \right) \Big|_{\partial\Omega} = I(z),$$

and $\psi(z)$ now can be recovered, up to an arbitrary additive constant, by solving the Neumann problem

$$\begin{cases} \Delta\psi(x) = 0, & x \in \Omega \\ \frac{\partial}{\partial n}\psi(z) = I(z) - n \cdot \left(\nabla \times \int_{\Omega} \frac{C(y)}{4\pi(z-y)} dy \right), & z \in \partial\Omega. \end{cases} \quad (26)$$

Now $J_I(x)$ is uniquely defined by the formula

$$J_I(x) = \nabla \times \int_{\Omega} \frac{C(y)}{4\pi(x-y)} dy + \nabla\psi(x), \quad x \in \Omega. \quad (27)$$

Proposition 3 *Under smoothness assumption of Proposition 1 current $J_I(x)$ is given by the formula (27), where function $\psi(x)$ is the (classical) solution of the Neumann problem (26).*

2.2.2 Other possibilities

If in addition to the curl $\nabla \times J_I(x)$, the surface term (equation (22)) has been reconstructed, there is no need to solve the Neumann problem. Instead, function $\Psi(x)$ is given explicitly by the following formula [31]:

$$\Psi(x) = \nabla_x \times \int_{\partial\Omega} \frac{J_I(y) \times n(y)}{4\pi(x-y)} dA(y).$$

The final expression for current J_I can now be written as

$$\begin{aligned} J_I(x) &= \nabla_x \times \left[\int_{\Omega} \frac{C(y)}{4\pi(x-y)} dy + \int_{\partial\Omega} \frac{J_I(y) \times n(y)}{4\pi(x-y)} dA(y) \right] \\ &= \nabla_x \times \int_{\bar{\Omega}} \frac{C(y) + J_I(y) \times n(y) \delta_{\partial\Omega}(y)}{4\pi(x-y)} dy, \quad x \in \Omega, \end{aligned} \quad (28)$$

where $\bar{\Omega}$ is the closure Ω . The term with the delta-function in the numerator of (28) coincides with the surface term given by equation (22). In order to avoid the direct numerical reconstruction of the singular term, one may want to try to modify the utilized TAT reconstruction algorithm so as to recover directly the convolution with $\frac{1}{4\pi|x|}$ contained in equation (28). The practicality of such an approach requires further investigation.

Finally, in certain simple domains one can find a way to solve the equation

$$C = \nabla \times J_I$$

for J_I in such a way as to explicitly satisfy boundary conditions (25) and thus to avoid the need of solving the Neumann problem (26). One such domain is a cube; we present the corresponding algorithm in Section 3.

2.3 Reconstructing the conductivity

In order to reconstruct the conductivity we will utilize three currents $J^{(k)}$, $k = 1, 2, 3$, corresponding to three different boundary conditions I_k . As we mentioned before we are using three different magnetic inductions $B^{(j)}$, $j = 1, 2, 3$. As a result, we obtain the values of the following measuring functionals $M_{I_k, B^{(j)}}(y, t)$

$$M_{I_k, B^{(j)}}(y, t) = \int_{\partial\Omega} I_k(z) u_{(j)}(z, t) dA(z), \quad j = 1, 2, 3, \quad k = 1, 2, 3, \quad (29)$$

where $u_{(j)}(z, t)$ is the electric potential corresponding to the acoustic wave with the velocity potential $\varphi(x, z, t)$ propagating through the body in the presence of constant magnetic field $B^{(j)}$. Notice that the increase in the number of currents $J^{(k)}$ does not require additional physical measurements: the same measured boundary values of $u_{(j)}(z, t)$ are used to compute different measuring functionals by changing the integration weight $I_k(z)$ in equation (4).

For each of the currents $J^{(k)}$ we apply one of the above-mentioned TAT reconstruction techniques to compute $\frac{\partial}{\partial t} M_{I_k, B^{(j)}}(y, 0)$. The knowledge of the latter functions for $B^{(j)}$, $j = 1, 2, 3$, allows us to recover the curls $C^{(k)} = \nabla \times J^{(k)}$, $k = 1, 2, 3$, (equation (21)) and, possibly, the surface terms (22). Finally, currents $J^{(k)}$ are reconstructed by one of the methods described in the previous section.

At the first sight, finding $\sigma(x)$ from the knowledge of $J^{(k)} = \sigma \nabla w_{I_k}$, $k = 1, 2, 3$, is a non-linear problem, since the unknown electric potentials w_{I_k} depend on $\sigma(x)$. However, as shown below, this problem can be solved explicitly without a linearization or some other approximation. Indeed, for any $k = 1, 2, 3$, the following formula holds:

$$0 = \nabla \times \frac{J^{(k)}}{\sigma} = \left(\nabla \frac{1}{\sigma} \right) \times J^{(k)} + \frac{1}{\sigma} C^{(k)} = -\frac{1}{\sigma^2} (\nabla \sigma) \times J^{(k)} + \frac{1}{\sigma} C^{(k)}$$

so that

$$\nabla \ln \sigma(x) \times J^{(k)}(x) = C_J^{(k)}(x), \quad x \in \Omega, \quad k = 1, 2, 3.$$

Now one can try to find $\nabla \ln \sigma$ at each point in Ω by solving the following (in general) over-determined system of linear equations:

$$\begin{cases} \nabla \ln \sigma \times J^{(1)} = C^{(1)} \\ \nabla \ln \sigma \times J^{(2)} = C^{(2)} \\ \nabla \ln \sigma \times J^{(3)} = C^{(3)} \end{cases} \quad (30)$$

Let us assume first, that currents $J^{(l)}(x)$, $l = 1, 2, 3$ form a basis in \mathbb{R}^3 at each point in Ω . There are 9 equations in system (30), whose unknowns are the three components of $\nabla \ln \sigma$, but the rank of the corresponding matrix does not exceed 6. In order to see this, let us multiply each equation of (30) by $J^{(l)}$, $l = 1, 2, 3$. (Since the three currents $J^{(l)}$ form a basis, this is equivalent to a multiplication by a non-singular matrix). We obtain

$$\begin{cases} \nabla \ln \sigma \cdot (J^{(1)} \times J^{(2)}) = C^{(1)} \cdot J^{(2)} \\ \nabla \ln \sigma \cdot (J^{(1)} \times J^{(2)}) = -C^{(2)} \cdot J^{(1)} \\ \nabla \ln \sigma \cdot (J^{(1)} \times J^{(3)}) = C^{(1)} \cdot J^{(3)} \\ \nabla \ln \sigma \cdot (J^{(1)} \times J^{(3)}) = -C^{(3)} \cdot J^{(1)} \\ \nabla \ln \sigma \cdot (J^{(2)} \times J^{(3)}) = C^{(2)} \cdot J^{(3)} \\ \nabla \ln \sigma \cdot (J^{(2)} \times J^{(3)}) = -C^{(3)} \cdot J^{(2)} \end{cases} \quad .$$

In the case of perfect measurements the right hand sides of equations number 2, 4, and 6 in the above system would coincide with those of equations 1, 3, and 5, respectively, and therefore the even-numbered equations could just be dropped from the system. However, in the presence of noise it is better to take the average of the equations with identical left sides, which is equivalent to finding the least squares solution of this system. We thus obtain:

$$\begin{cases} \nabla \ln \sigma \cdot (J^{(1)} \times J^{(2)}) = \frac{1}{2}(C^{(1)} \cdot J^{(2)} - C^{(2)} \cdot J^{(1)}) \\ \nabla \ln \sigma \cdot (J^{(1)} \times J^{(3)}) = \frac{1}{2}(C^{(1)} \cdot J^{(3)} - C^{(3)} \cdot J^{(1)}) \\ \nabla \ln \sigma \cdot (J^{(2)} \times J^{(3)}) = \frac{1}{2}(C^{(2)} \cdot J^{(3)} - C^{(3)} \cdot J^{(2)}) \end{cases} \quad (31)$$

After some simple linear algebra transformations (see Appendix) the solution of (31) can be written explicitly as follows:

$$\nabla \ln \sigma = \frac{1}{2J^{(1)} \cdot (J^{(2)} \times J^{(3)})} M \begin{pmatrix} C^{(2)} \cdot J^{(3)} - C^{(3)} \cdot J^{(2)} \\ -C^{(1)} \cdot J^{(3)} + C^{(3)} \cdot J^{(1)} \\ C^{(1)} \cdot J^{(2)} - C^{(2)} \cdot J^{(1)} \end{pmatrix}, \quad (32)$$

where M is (3×3) matrix whose columns are the Cartesian coordinates of the currents $J^{(l)}, l = 1, 2, 3$:

$$M = \begin{pmatrix} J^{(1)} & J^{(2)} & J^{(3)} \end{pmatrix}. \quad (33)$$

Since, by assumption, currents $J^{(l)}$ form a basis at each point of Ω , the denominator in (32) never vanishes and, thus, equation (32) can be used to reconstruct $\nabla \ln \sigma$ in all of Ω . Finally, we compute the divergence of both sides in (32):

$$\Delta \ln \sigma = \frac{1}{2} \nabla \cdot \left[\frac{1}{J^{(1)} \cdot (J^{(2)} \times J^{(3)})} M \begin{pmatrix} C^{(2)} \cdot J^{(3)} - C^{(3)} \cdot J^{(2)} \\ -C^{(1)} \cdot J^{(3)} + C^{(3)} \cdot J^{(1)} \\ C^{(1)} \cdot J^{(2)} - C^{(2)} \cdot J^{(1)} \end{pmatrix} \right], \quad (34)$$

and solve the above Poisson equation for $\ln \sigma$ in Ω subject to the Dirichlet boundary conditions

$$\ln \sigma|_{\partial\Omega} = 0. \quad (35)$$

The above reconstruction procedure works if currents $J^{(1)}$, $J^{(2)}$, and $J^{(3)}$ are linearly independent at each point in Ω . For an arbitrary conductivity σ this cannot be guaranteed. There exists a counterexample [8] describing such a conductivity for which a boundary condition can be found such that the corresponding current vanishes at a certain point within the domain. Clearly, while such a situation can occur, it is unlikely to occur for an arbitrary conductivity σ , and our method should still be useful in practice.

Moreover, the condition of the three currents forming a basis at each point in space can be relaxed. Below we show that if only one of the currents $J^{(1)}$, $J^{(2)}$, and $J^{(3)}$ vanishes (say, $J^{(3)} = 0$) at some point and the two other currents are not parallel, the following truncated system is still uniquely solvable:

$$\begin{cases} \nabla \ln \sigma \times J^{(1)} = C^{(1)} \\ \nabla \ln \sigma \times J^{(2)} = C^{(2)} \end{cases} \quad (36)$$

Indeed, let us multiply via dot product the above equations by $J^{(2)}$ and $J^{(1)}$ respectively, and subtract them. We obtain

$$\nabla \ln \sigma \cdot (J^{(1)} \times J^{(2)}) = \frac{1}{2} (C^{(1)} \cdot J^{(2)} - C^{(2)} \cdot J^{(1)}). \quad (37)$$

Now, multiply the first equation in (36) by $J^{(1)} \times J^{(2)}$. The left hand side will take the form

$$\begin{aligned} (\nabla \ln \sigma \times J^{(1)}) \cdot (J^{(1)} \times J^{(2)}) &= \nabla \ln \sigma \cdot [J^{(1)} \times (J^{(1)} \times J^{(2)})] \\ &= \nabla \ln \sigma \cdot [(J^{(1)} \cdot J^{(2)}) J^{(1)} - (J^{(1)} \cdot J^{(1)}) J^{(2)}], \end{aligned}$$

which leads to the equation

$$\nabla \ln \sigma \cdot [(J^{(1)} \cdot J^{(2)}) J^{(1)} - (J^{(1)} \cdot J^{(1)}) J^{(2)}] = C^{(1)} \cdot (J^{(1)} \times J^{(2)}). \quad (38)$$

Similarly, by multiplying the second equation in (36) by $(J^{(2)} \times J^{(1)})$ we obtain

$$\nabla \ln \sigma \cdot [(J^{(1)} \cdot J^{(2)}) J^{(2)} - (J^{(2)} \cdot J^{(2)}) J^{(1)}] = C^{(2)} \cdot (J^{(2)} \times J^{(1)}). \quad (39)$$

Equations (37), (38) and (39) form a linear system with three equations and three unknowns. In order to show that the matrix of this system is non-singular, it is enough to show that the vectors given by the bracketed expressions in (38) and (39) are not parallel. The cross-product of these terms yields

$$[\dots] \times [\dots] = (J^{(1)} \times J^{(2)}) \left[(J^{(1)} \cdot J^{(2)})^2 - (J^{(1)} \cdot J^{(1)}) (J^{(2)} \cdot J^{(2)}) \right].$$

The above expression is clearly non-zero if $J^{(1)}$ and $J^{(2)}$ are not parallel, and therefore the system of the three equations (37), (38), (39) is uniquely solvable in this case.

Theorem 4 *Suppose that the conditions of Proposition 1 are satisfied, and that the conductivity $\sigma(x)$ and boundary currents I_k , $k = 1, 2, 3$, are such that at each point $x \in \Omega$ two of the three correspondent currents $J^{(k)}$ are non-parallel. Then the logarithm of the conductivity $\ln \sigma$ is uniquely determined by the values of the measuring functionals $M_{I_k, B^{(j)}}(y, t)$, $k = 1, 2, 3$, $j = 1, 2, 3$, $y \in \Sigma$ and $t \in [0, D_{\max}/c]$.*

Proof. By Propositions 1, 2, 3, and 4, from the values of $M_{I_k, B^{(j)}}(y, t)$ one can reconstruct currents $J^{(k)}(x)$, $k = 1, 2, 3$, at each point x in Ω . Since at each point at least two of the three currents (lets call them $J^{(1)}$, and $J^{(2)}$) are not parallel, system of the three equations (37), (38), (39) is uniquely solvable, and $\nabla \ln \sigma$ can be found at each point in Ω . Since it was assumed that σ is bounded away from zero, $\nabla \ln \sigma$ is a C^∞ function in Ω . By computing the divergence of $\nabla \ln \sigma$ the problem of finding $\ln \sigma$ reduces to solving the Poisson problem with zero Dirichlet boundary conditions in a smooth domain Ω . ■

The condition that out of the three currents two are non-zero and not parallel, is less restrictive than the requirement that the three currents are linearly independent. To the best of our knowledge, there exists no counterexample showing that the former condition can be violated, i.e. that one of the three currents generated by linearly independent boundary conditions vanishes and the other two are parallel at some point in space. On the other hand, we know of no proof that this cannot happen.

3 The case of a rectangular domain

In the previous section we presented a theoretical scheme for finding the currents $J^{(k)}$, $k = 1, 2, 3$, and conductivity $\sigma(x)$ from the MAET measurements in a rather general setting, where the electrical domain Ω and surface Σ supporting the acoustic sources are quite arbitrary. This scheme consists of several steps including the solution of the inverse problem of TAT in the domain surrounded by Σ , solution of the Neumann problem for the Laplace equation in Ω , and solution of the Poisson equation in Ω for $\ln \sigma$. All these problems are well-studied and various algorithms for their numerical solution are well known. However, in the simplest case when Ω is a cube and Σ coincides with $\partial\Omega$, the reconstruction can be obtained by means of an explicit series solution as described below.

3.1 Fast reconstruction algorithm

Let us assume that the domain Ω is a cube $[0, 1] \times [0, 1] \times [0, 1]$, and the sound sources are located on $\partial\Omega$. (In practice such a measuring configuration will occur if the object is placed in a cubic tank filled with conductive liquid, and the sound sources and electrical connections are placed on the tank walls). We will use three boundary conditions I_k defined by the formulae:

$$I_k(x) = \begin{cases} \frac{1}{2}, & x \in \partial\Omega, \quad x_k = 1 \\ -\frac{1}{2}, & x \in \partial\Omega, \quad x_k = 0 \\ 0, & x \in \partial\Omega, \quad 0 < x_k < 1 \end{cases}, \quad k = 1, 2, 3, \quad x = (x_1, x_2, x_3). \quad (40)$$

As before, all the measurements are repeated with three different direction of the magnetic field $B^{(j)} = |B|e_j$, $j = 1, 2, 3$, and the values of functionals $M_{I_k, B^{(j)}}(y, t)$ (see equation (29)) are computed from the measurements of the electrical potentials $u^{(j)}(x, t)$ on $\partial\Omega$, for $t \in [0, \frac{\sqrt{3}}{c}]$.

We start the reconstruction by applying to $M_{I_k, B^{(j)}}(y, t)$ the fast cubic-domain TAT algorithm [21] to recover the regular terms $M_{I^{(k)}, B^{(j)}}^{\text{reg}}(x, 0)$, $j = 1, 2, 3$, $k = 1, 2, 3$. (The algorithm we chose automatically sets to zero the sources corresponding to the surface terms $\frac{\partial}{\partial t} M_{I^{(k)}, B^{(j)}}^{\text{sing}}(x, 0)$ supported on Σ). This is done for all three directions of $B^{(j)}$, so that we immediately obtain the curls $C^{(k)}(x) = \nabla \times J^{(k)}(x)$, $k = 1, 2, 3$, $x \in \partial\Omega$.

Now, since the currents are divergence-free,

$$\nabla \times C^{(k)}(x) = \nabla \times \nabla \times J^{(k)}(x) = -\Delta J^{(k)}(x),$$

and we can try to solve the above equation as a set of Poisson problems for the components $J^{(k)}(x)$ in Ω . Below we discuss how to enforce the correct boundary conditions for these Poisson problems.

Let us recall that

$$J^{(k)}(x) = \sigma \nabla w^{(k)}(x),$$

where $w^{(k)}(x)$ is the corresponding electric potential. It is convenient to subtract the linear component of potentials, i.e. to introduce potentials $w^{(k),0}(x)$ and $J^{(k),0}(x)$ defined as follows:

$$\begin{aligned} w^{(k)}(x) &= w^{(k),0}(x) + x_k, \\ J^{(k)}(x) &= J^{(k),0}(x) + e_k, \quad k = 1, 2, 3. \end{aligned}$$

Now each $w^{(k),0}(x)$ satisfies zero Neumann conditions on $\partial\Omega$, and thus can be extended by even reflections to a periodic function in \mathbb{R}^3 . Since $w^{(k),0}(x)$ is a harmonic function near $\partial\Omega$, such an extension would be a harmonic function in the neighborhood of $\partial\Omega$ and its reflections. Therefore, each $w^{(k),0}(x)$ can be expanded in the Fourier cosine series in Ω , and the derivatives of this series yield correct behavior of the so-computed $\nabla w^{(k),0}(x)$ on $\partial\Omega$, and also of currents $J^{(k),0}(x)$ (the latter currents coincide with $\nabla w^{(k),0}(x)$ in the vicinity of $\partial\Omega$). Therefore, the components of currents $J^{(k),0}(x)$ should be expanded in the Fourier series whose basis functions are the corresponding derivatives of the cosine series. In other words, the following series yield correct boundary conditions when used as a basis for expanding currents $J^{(k),0}(x)$, $k = 1, 2, 3$:

$$\begin{cases} J_1^{(k),0}(x) = \sum_{l=1}^{\infty} \sum_{m=0}^{\infty} \sum_{n=0}^{\infty} A_{l,m,n}^{(k),1} \sin \pi l x_1 \cos \pi m x_2 \cos \pi n x_3 \\ J_2^{(k),0}(x) = \sum_{l=0}^{\infty} \sum_{m=1}^{\infty} \sum_{n=0}^{\infty} A_{l,m,n}^{(k),2} \cos \pi l x_1 \sin \pi m x_2 \cos \pi n x_3 \\ J_3^{(k),0}(x) = \sum_{l=0}^{\infty} \sum_{m=0}^{\infty} \sum_{n=1}^{\infty} A_{l,m,n}^{(k),3} \sin \pi l x_1 \cos \pi m x_2 \sin \pi n x_3 \end{cases}, \quad (41)$$

where $J^{(k),0}(x) = (J_1^{(k),0}(x), J_2^{(k),0}(x), J_3^{(k),0}(x))$. Now, since $\nabla \times J^{(k),0}(x) = \nabla \times J^{(k)}(x)$:

$$\Delta J^{(k),0}(x) = -\nabla \times C^{(k)}(x), \quad k = 1, 2, 3 \quad (42)$$

and, if the Poisson problems (42) are solved for each component of $J^{(k),0}$ using sine/cosine Fourier series (41), the correct boundary conditions will be attained. The computation can be performed efficiently using the Fast Fourier sine and cosine transforms (FFST and FFCT).

One can notice that before Poisson problems (42) can be solved, the curl of the $C^{(k)}(x)$ needs to be computed. We compute it by expanding $C^{(k)}(x)$ in the Fourier sine series and by differentiating the series, again using FFST and FFCT. This computation amounts to numerical differentiation of the data that may contain a significant amount of noise. However, this does not give rise to instabilities, since this differentiation is immediately followed by an inverse Laplacian (describing solution of the Poisson problem), so that the combined operator is actually smoothing.

Finally, once the currents are reconstructed, we form the right hand side of the system (34) and solve this Poisson problem for $\ln \sigma(x)$ by using the Fourier sine series which yields the desired boundary conditions (35). Again, FFST and FFCT are utilized here and in the computations of the divergence needed to form equation (34).

One could notice that all the steps of the present algorithm are explicit, and can be performed using FFST and FFCT, so that the number of floating point operations (flops) required to complete the computations is $O(n^3 \ln n)$ for a $(n \times n \times n)$ computational grid. The same is true for the TAT reconstruction technique [21] used on the first step of computations, so that the whole method is fast; it has complexity of $O(n^3 \ln n)$ flops.

3.2 Numerical results

Since the author does not have at his disposal any real MAET measurements, the work of the present reconstruction algorithm (for a cubic domain) will be demonstrated on simulated

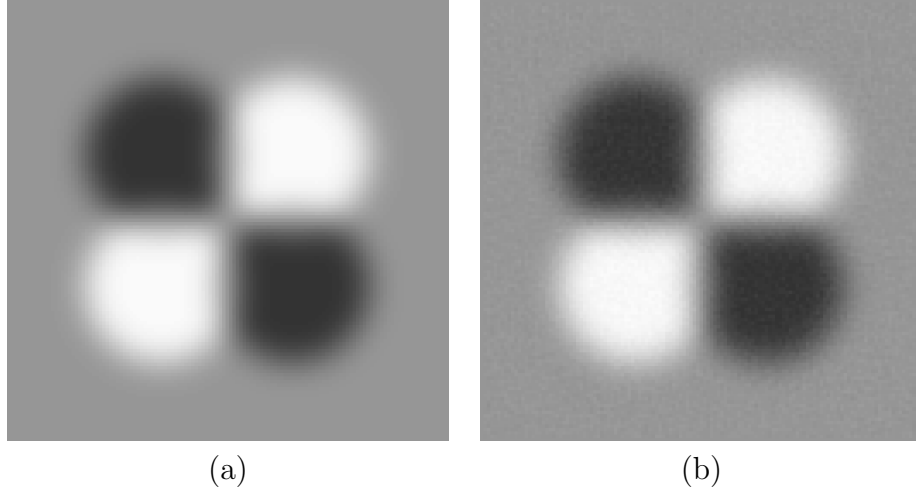


Figure 1: A 3D simulation with a smooth phantom representing $\ln \sigma(x)$
(a) the cross section of the phantom by the plane $x_3 = 0.5$
(b) reconstruction from the data with added 50% (in L_2 sense) noise

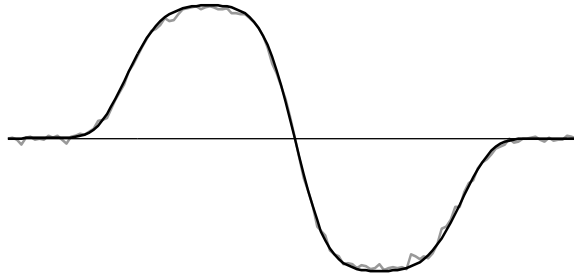


Figure 2: The cross section of the reconstructed image (shown in Figure 1) by the line $x_1 = 0.25, x_3 = 0.5$. The thick black line represents the phantom, the gray line corresponds to the reconstructed image

data. The most thorough simulation would entail solving equation (2) with the boundary conditions (3) for various velocity fields $V(x, t)$ corresponding to the propagating spherical fronts originating at different locations on $\partial\Omega$. For a good reconstruction, the number of the data points should be comparable with the number of unknowns. We would like to reconstruct the conductivity on a fine 3D grid (say, of the size $257 \times 257 \times 257$), which implies having several millions of unknowns. Thus, we would need to solve equation (2) several million times. This task is too challenging computationally.

Instead, for a given phantom and for the set of functions $I^{(k)}$ given by equations (40) we computed currents $J^{(k)}$ by solving equation (5) with boundary conditions (6). Next, the wave equation (14) with the initial condition $h(y) = B^{(j)} \cdot \nabla \times J^{(k)}(x)$ was solved for $j = 1, 2, 3, k = 1, 2, 3$; the values of the solution of this equation at points in $\partial\Omega$ simulated the regular part $\rho M_{I,B}^{\text{reg}}(x, t)$ of the measuring functionals $\rho M_{I,B}(y, t)$. Note that for simplicity we did not model the singular term $M_{I,B}^{\text{sing}}(x, t)$ given by (15). Theoretically, when the TAT

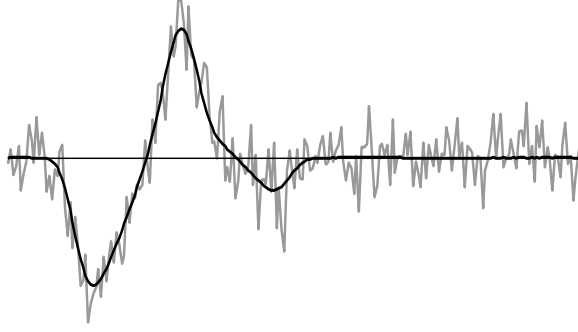


Figure 3: Plot of one of the simulated measurement functionals for one of the detector positions (see text for details): thick black line represents accurate values, gray line shows the data with added 50% noise

reconstruction algorithm [21] is applied to such data, since this term is not supported in Ω it will not contribute to the reconstruction, and so the additional effort to simulate it would not be rewarded with additional insight.

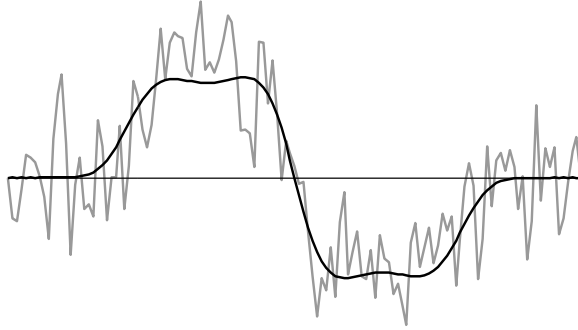


Figure 4: Profile of the reconstructed curl (gray line) compared to the accurate values (thick black line). Shown are the values of the third component of $C^{(1)}$ along the line $x_2 = 0.5$, $x_3 = 0.5$

As the first phantom simulating $\ln \sigma(x)$ we used the following linear combinations of four C^8 radially symmetric functions $\varphi(x - x^{(i)})$ with centers $x^{(i)}$ lying in the plane $x_3 = 0$:

$$f(x) = \sum_{i=1}^4 a_i \varphi(|x - x^{(i)}|),$$

$$\begin{aligned} x^{(1)} &= (0.25, 0.25, 0), & a_1 &= 0.5, \\ x^{(2)} &= (0.25, 0.75, 0), & a_2 &= -0.5, \\ x^{(3)} &= (0.75, 0.25, 0), & a_3 &= -0.5, \\ x^{(4)} &= (0.75, 0.75, 0), & a_4 &= 0.5, \end{aligned}$$

where $\varphi(t)$ is a decreasing non-negative trigonometric polynomial on $[0, r_0]$, such that $\varphi(0) =$

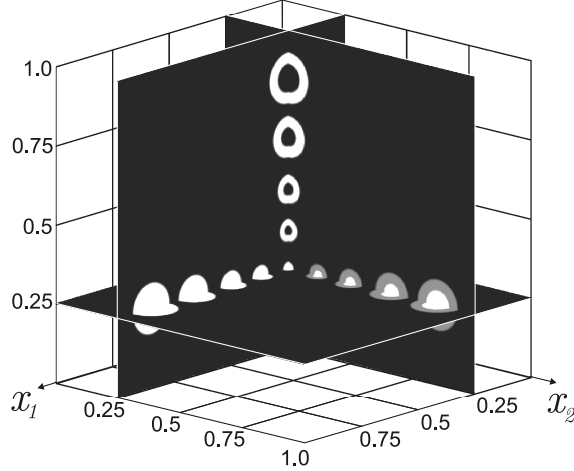


Figure 5: The second, (almost) piece-wise constant 3D phantom. Shown are cross sections by the planes $x_j = 0.25$, $j = 1, 2, 3$

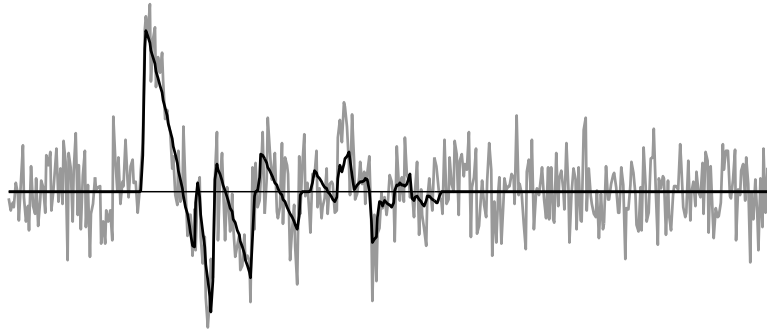


Figure 6: Plot of the values of one of the simulated measurement functionals for one of the detector positions (see text for details): thick black line represents accurate values, gray line shows the data with added 100% noise

1, $\varphi(t) = 0$ for $t \geq r_0$ and the first eight derivatives of φ vanish at 0 and at r_0 . Radius r_0 was equal to 0.34 in this simulation. A gray scale picture of this phantom is shown in Figure 1(a). Figure 1(b) demonstrates the cross-section by the plane $x_3 = 0.5$ of the image reconstructed on a $129 \times 129 \times 129$ computational grid from simulated MAET data with added simulated noise. The acoustic sources were located at the nodes of 129×129 Cartesian grids on each of the six faces of cubic domain Ω . For each source 223 values of each of the measuring functionals were computed, representing 223 different time samples or, equivalently, 223 different radii of the propagating acoustic front.

The measurement noise was simulated by adding values of uniformly distributed random variable to the data. The so-simulated noise was scaled in such a way that for each time series (one source position) the noise intensity in L^2 norm was 50% of the intensity of the signal (i.e. of the L^2 norm of the data sequence representing the measuring functional). In spite of such high level of noise in the data, the reconstructed image shown in Figure 1(b)

contains very little noise. This can also be verified by looking at the plot of the cross section of the latter image along the line $x_2 = 0.25$, presented in Figure 2.

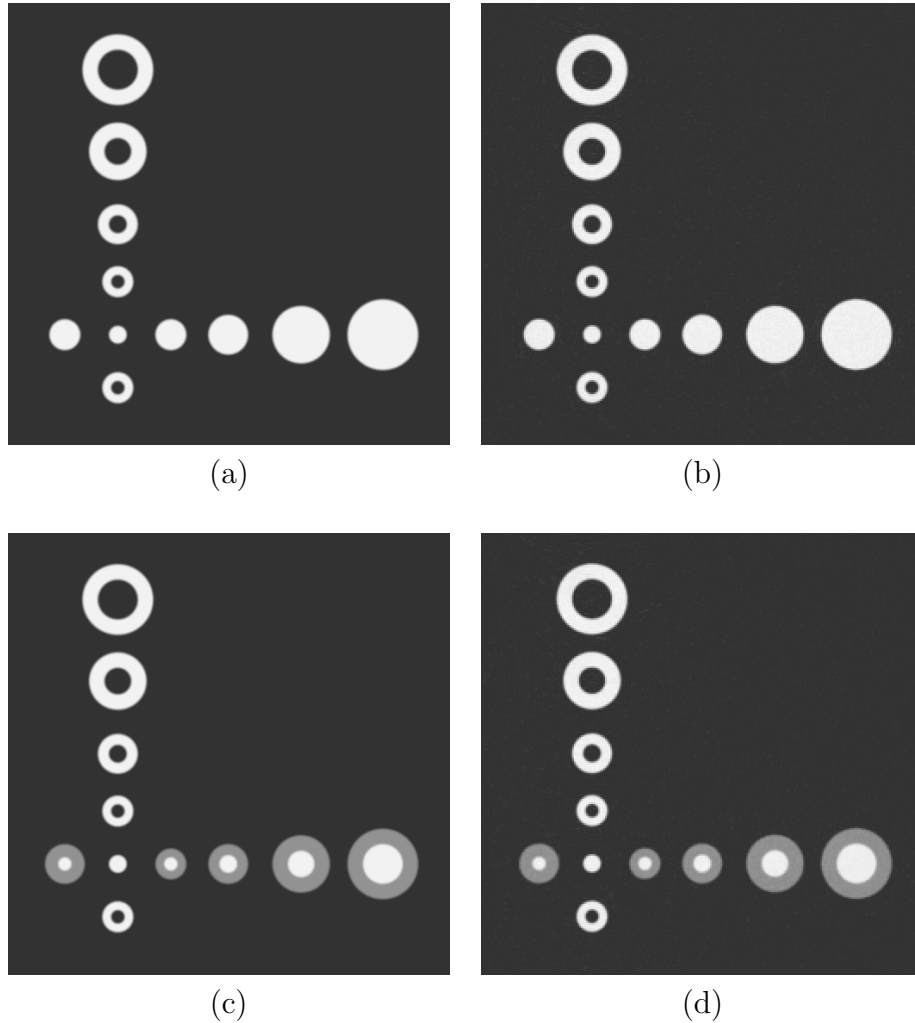


Figure 7: Simulation in $3D$ with phantom shown in Figure 5; (a) and (c) are the cross sections of the phantom by planes $x_2 = 0.25$ and $x_1 = 0.25$, respectively; (b) and (d) are the corresponding cross sections of the reconstruction from the data with added 100% (in L_2 sense) noise

In order to better understand the origins of such unusually low noise sensitivity, we plot in Figure 3 a profile of one of the time series, $M_{I,B(3)}(y, t)$ for point $y = (1, 0.5, 0.5)$. The thick black line represents the accurate measurements, the gray line shows the with the added noise. In Figure 4 we plot a profile of the reconstructed curl $C^{(1)}(x)$ (gray line) against the correct values (black line). (This plot corresponds to the cross-section of the third component of $C^{(1)}$ along the line $x_2 = 0.5$, $x_3 = 0.5$). The latter figure shows that noise is amplified during the first step of the reconstruction (inversion of the spherical mean Radon transform). This is to be expected, since the corresponding inverse problem is mildly ill-posed, similarly to the inversion of the classical Radon transform. However, on the second

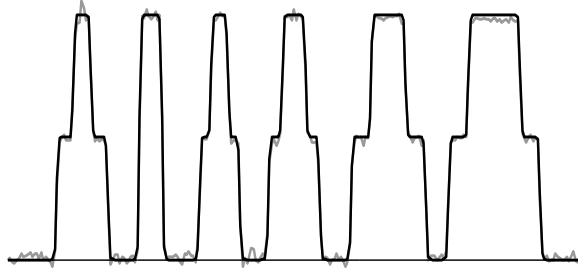


Figure 8: The cross section of the reconstructed image by the line $x_1 = 0.25$, $x_3 = 0.25$. The thick black line represents the phantom, the gray line corresponds to the image reconstructed from the data with added 100% (in L^2 sense) noise

step of the reconstruction, corresponding to solving the problem (34), the noise is significantly smoothed out. This is not surprising, since the corresponding operator is a smoothing one. As a result, we obtain the low-noise image shown in Figure 1(b).

The second simulation we report used an (almost) piece-wise constant phantom of $\ln \sigma(x)$ modeled by a linear combination of several slightly smoothed characteristic functions of balls of different radii. The centers of the balls were located on the pair-wise intersections of planes $x_1 = 0.25$, $x_2 = 0.25$, $x_3 = 0.25$, as shown in Figure 5. The minimum value of $\ln \sigma(x)$ in this phantom was 0 (dark black color), the maximum value is 1 (white color). The simulated MAET data corresponded to the acoustic sources located at the nodes of 257×257 Cartesian grids on each of the six faces of cubic domain Ω . For each source, a time series consisting of 447 values for each measuring functional were simulated. In order to model the noise, to each of the time series we added a random sequence scaled so that the L^2 norm of the noise was equal to that of the signal (i.e. 100% noise was applied).

In Figure 6 we present the profile of the time series $M_{I_1, B^{(3)}}(y, t)$ for the point $y = (1, 0.5, 0.5)$. As before, the thick black line represents the accurate measurements, and the gray line shows the data with added noise.

The reconstruction was performed on the grid of size $257 \times 257 \times 257$. The cross sections of the reconstructed image by planes $x_1 = 0.25$ and $x_2 = 0.25$ are shown in the Figure 7(b) and (d), next to the corresponding images of the phantom (i.e. parts (a) and (c) of the latter figure). The cross section profile of the image shown in part (d), corresponding to the line $x_1 = 0.25$, $x_3 = 0.25$, is plotted in Figure 8.

As in the first simulation, we obtain a very accurate reconstruction with little noise. This is again the result of a smoothing operator applied when the Poisson problem is solved on the last step of the algorithm. An additional improvement in the quality of the image comes from the rather singular nature of the second phantom. Indeed, while the noise is more or less uniformly distributed over the volume of the cubic domain, the signal (the non-zero $\ln \sigma$) is supported in a rather small fraction of the volume, thus increasing the visual contrast between the noise and the signal.

Final remarks and conclusions

Mathematical model

In Section 1 we presented a mathematical model describing the MAET measurements. In general, it agrees with the model used in [13, 30]. However, instead of point-wise electrical boundary measurements we consider a more general scheme. The advantage of such an approach is generality and ease of analysis and numerical modeling. In particular, it contains as a partial case the pointwise measurement of electrical potentials (reported in [13, 30]).

Another novel element in this model is the use of velocity potentials which allow us to simplify analysis and obtain a better understanding of the problem at hand. We discussed in detail the case of acoustic signal presented by propagating acoustic fronts from small sources. However, the same mathematics can be used to model time-harmonic sources. Since the problem is linear with respect to the velocity potential, the connection between the two problems is through the direct and inverse Fourier transforms of the data in time. Finally, plane wave irradiation (considered for example in [30]) is a partial case of irradiation by time harmonic sources, when they are located far away from the object.

General reconstruction scheme

In Section 2 we presented a general scheme for the solution of the inverse problem of MAET obtained under the assumption of propagating spherical acoustic fronts. (As we mentioned above, a slight modification of this scheme would allow one to utilize time harmonic sources and plane waves instead of the fronts we used). The scheme consists of the following steps:

1. Apply one of the suitable TAT reconstructions techniques to measuring functionals $M_{I^{(k)}, B^{(j)}}(y, t)$, $j, k = 1, 2, 3$, to reconstruct the regular terms $M_{I^{(k)}, B^{(j)}}^{\text{reg}}(x, t)$ at $t = 0$ and thus to obtain the curls of $J^{(k)}$.
2. Compute currents $J^{(k)}$ from their curls (this step may require solving the Neumann problem for the Laplace equation)
3. Find $\nabla \ln \sigma$ at each point in Ω using formula (32) or by solving system of equations (37), (38), (39).
4. Find values of $\Delta \ln \sigma$ by computing the divergence of $\nabla \ln \sigma$.
5. Compute $\ln \sigma$ by solving the Poisson problem with the zero Dirichlet boundary conditions.

Theoretical properties and numerical methods for all three steps are well known. The first step is mildly ill-posed (similar to the inversion of the classical Radon transform), the second step is stable, and the third step is described by a smoothing operator. Our rather informal discussion suggests that the total reconstruction procedure is stable (it does not exhibit even the mild instability present in classical computer tomography), and our numerical experiments confirm this assertion. We leave a rigorous proof of this conjecture for the future work.

Comparison with AEIT

MAET is similar to AET in that it seeks to overcome the instability of EIT by adding the ultrasound component to the electrical measurements. However, MAET has some advantages:

1. The arising problem is linear and can be solved explicitly.
2. The AEIT measurements seem to produce a very weak signal; successful acquisition of such signals in a realistic measuring configuration have not been reported so far. The signal in MAET is stronger; in fact, first reconstructions from real measurements have already been obtained [13].

The case of a rectangular domain

In Section 3 we presented a completely explicit set of formulae that yield a series solution of the MAET problem for the case of the cubic domain. It reduces the problem to a set of sine and cosine Fourier transforms, and thus, it can be easily implemented using FFTs. This, in turn, results in a fast algorithm that requires $\mathcal{O}(n^3 \ln n)$ floating point operations to complete a reconstructions on a $n \times n \times n$ Cartesian grid.

Feasibility of reconstruction using two directions of B

It is theoretically possible to shorten the potentially long acquisition time by reducing the number of different directions of B . If only two orthogonal directions of magnetic field B are used, only two components of a curl $C = \nabla \times J_I$ will be reconstructed on the first step of our method (say C_1 and C_2). However, since $\operatorname{div} \operatorname{curl} J = 0$,

$$\frac{\partial}{\partial x_3} C_3 = -\frac{\partial}{\partial x_1} C_1 - \frac{\partial}{\partial x_2} C_2.$$

Since C vanishes on $\partial\Omega$, the above equation can be integrated in x_3 , and thus C_3 can be reconstructed from C_1 and C_2 . A further study is needed to see how much this procedure would affect the stability of the whole method.

Acknowledgements

The author gratefully acknowledges support by the NSF through the DMS grant 0908208.

Appendix

Consider the following system of linear equations

$$\begin{cases} X \cdot (A \times B) = R_1 \\ X \cdot (A \times C) = R_2 \\ X \cdot (B \times C) = R_3 \end{cases} \quad (43)$$

where A , B , and C are given linearly independent vectors from \mathbb{R}^3 , $X \in \mathbb{R}^3$ is the vector of unknowns, and R_j , $j = 1, 2, 3$, are given numbers. The first equation can be re-written in the following form

$$R_1 = \begin{vmatrix} x_1 & x_2 & x_3 \\ a_1 & a_2 & a_3 \\ b_1 & b_2 & b_3 \end{vmatrix} = \begin{vmatrix} x_1 & a_1 & b_1 \\ x_2 & a_2 & b_2 \\ x_3 & a_3 & b_3 \end{vmatrix} = \begin{vmatrix} x_1 & b_1 & c_1 \\ x_2 & b_2 & c_2 \\ x_3 & b_3 & c_3 \end{vmatrix}$$

or

$$r_1 = \frac{1}{\det M} \begin{vmatrix} x_1 & b_1 & c_1 \\ x_2 & b_2 & c_2 \\ x_3 & b_3 & c_3 \end{vmatrix}, \quad (44)$$

where M is a (3×3) matrix whose columns are vectors A , B , and C , and $r_1 = R_1/\det M$. Similarly,

$$r_2 = \frac{1}{\det M} \begin{vmatrix} a_1 & x_1 & c_1 \\ a_2 & x_2 & c_2 \\ a_3 & x_3 & c_3 \end{vmatrix}, \quad (45)$$

and

$$r_3 = \frac{1}{\det M} \begin{vmatrix} x_1 & b_1 & c_1 \\ x_2 & b_2 & c_2 \\ x_3 & b_3 & c_3 \end{vmatrix}, \quad (46)$$

where $r_2 = -R_2/\det M$ and $r_3 = R_3/\det M$. Formulae (44)-(46) can be viewed as the solution of the following system of equations obtained using Cramer's rule:

$$\begin{pmatrix} a_1 & b_1 & c_1 \\ a_2 & b_2 & c_2 \\ a_3 & b_3 & c_3 \end{pmatrix} \begin{pmatrix} r_3 \\ r_2 \\ r_1 \end{pmatrix} = \begin{pmatrix} x_1 \\ x_2 \\ x_3 \end{pmatrix}.$$

Therefore, solution of system (43) is given by the formula

$$X = \frac{1}{\det M} \begin{pmatrix} a_1 & b_1 & c_1 \\ a_2 & b_2 & c_2 \\ a_3 & b_3 & c_3 \end{pmatrix} \begin{pmatrix} R_3 \\ -R_2 \\ R_1 \end{pmatrix}.$$

In addition, $\det M = A \cdot (B \times C)$.

References

- [1] M. Agranovsky and P. Kuchment, Uniqueness of reconstruction and an inversion procedure for thermoacoustic and photoacoustic tomography with variable sound speed, *Inverse Problems* **23** (2007) 2089–102.
- [2] G. Ambartsoumian and S. Patch, Thermoacoustic tomography: numerical results. Proceedings of SPIE 6437 *Photons Plus Ultrasound: Imaging and Sensing 2007: The Eighth Conference on Biomedical Thermoacoustics, Optoacoustics, and Acousto-optics*, (2007) Alexander A. Oraevsky, Lihong V. Wang, Editors, 64371B.
- [3] H. Ammari, E. Bonnetier, Y. Capdeboscq, M. Tanter, and M. Fink, Electrical impedance tomography by elastic deformation, *SIAM J. Appl. Math.* **68** (2008) 1557–1573.
- [4] H. Ammari, Y. Capdeboscq, H. Kang, and A. Kozhemyak, Mathematical models and reconstruction methods in magneto-acoustic imaging, *Euro. Jnl. of Appl. Math.*, **20** (2009) 303–17.
- [5] D. C. Barber, B. H. Brown, Applied potential tomography, *J. Phys. E.: Sci. Instrum.* **17** (1984), 723–733.
- [6] L. Borcea, Electrical impedance tomography, *Inverse Problems* **18** (2002) R99–R136.
- [7] P. Burgholzer, G. J. Matt, M. Haltmeier, and G. Paltauf, Exact and approximative imaging methods for photoacoustic tomography using an arbitrary detection surface, *Phys Review E*, **75** (2007) 046706.
- [8] Y. Capdeboscq, J. Fehrenbach, F. de Gournay, O. Kavian, Imaging by modification: numerical reconstruction of local conductivities from corresponding power density measurements, *SIAM J. Imaging Sciences*, **2/4** (2009) 1003–1030.
- [9] M. Cheney, D. Isaacson, and J. C. Newell, Electrical Impedance Tomography, *SIAM Review*, **41**, (1999) 85–101.
- [10] D. Colton and R. Kress, *Inverse acoustic and electromagnetic scattering theory*, Springer-Verlag (2001).
- [11] D. Finch, S. Patch and Rakesh, Determining a function from its mean values over a family of spheres, *SIAM J. Math. Anal.*, **35** (2004) 1213–40.
- [12] D. Gilbarg and N. S. Trudinger, *Elliptic Partial Differential Equations of Second Order*, Springer-Verlag (1983).
- [13] S. Haider, A. Hrbek, and Y. Xu, Magneto-acousto-electrical tomography: a potential method for imaging current density and electrical impedance, *Physiol. Meas.* **29** (2008) S41-S50.

- [14] Y. Hristova, P. Kuchment, and L. Nguyen, On reconstruction and time reversal in thermoacoustic tomography in homogeneous and non-homogeneous acoustic media, *Inverse Problems*, **24**: 055006, 2008.
- [15] R. A. Kruger, P. Liu, Y. R. Fang, and C. R. Appledorn, Photoacoustic ultrasound (PAUS) reconstruction tomography, *Med. Phys.*, **22** (1995) 1605–09.
- [16] R. A. Kruger, D. R. Reinecke, and G. A. Kruger, Thermoacoustic computed tomography - technical considerations, *Med. Phys.* **26** (1999) 1832–7.
- [17] P. Kuchment and L. Kunyansky, Mathematics of Photoacoustic and Thermoacoustic Tomography, Chapter 19, *Handbook of Mathematical Methods in Imaging*, Springer-Verlag, (2011) 819-865.
- [18] P. Kuchment and L. Kunyansky, Synthetic focusing in ultrasound modulated tomography, *Inverse Problems and Imaging*, **4** (2010) 665 – 673.
- [19] P. Kuchment and L. Kunyansky, 2D and 3D reconstructions in acousto-electric tomography, *Inverse Problems* **27** (2011) 055013.
- [20] L. Kunyansky, Explicit inversion formulae for the spherical mean Radon transform, *Inverse Problems*, **23** (2007) 737–783.
- [21] L. Kunyansky, A series solution and a fast algorithm for the inversion of the spherical mean Radon transform, *Inverse Problems*, **23** (2007) S11–S20.
- [22] L. Kunyansky, Reconstruction of a function from its spherical (circular) means with the centers lying on the surface of certain polygons and polyhedra, *Inverse Problems*, **27** (2011) 025012.
- [23] L. Kunyansky, Fast reconstruction algorithms for the thermoacoustic tomography in certain domains with cylindrical or spherical symmetries, Preprint (2011) Arxiv:Math.AP 1102.1413
- [24] L. Kunyansky and P. Kuchment, Synthetic focusing in Acousto-Electric Tomography, in *Oberwolfach Report* No. 18/2010 DOI: 10.4171/OWR/2010/18, Workshop: Mathematics and Algorithms in Tomography, Organised by Martin Burger, Alfred Louis, and Todd Quinto, April 11th – 17th, (2010) 44–47.
- [25] B. Lavandier, J. Jossinet and D. Cathignol, Experimental measurement of the acousto-electric interaction signal in saline solution, *Ultrasonics* **38** (2000) 929–936.
- [26] A. Montalibet, J. Jossinet, A. Matias, and D. Cathignol, Electric current generated by ultrasonically induced Lorentz force in biological media, *Med. Biol. Eng. Comput.* **39** (2001) 15–20.
- [27] S. J. Norton and M. Linzer, Ultrasonic reflectivity imaging in three dimensions: exact inverse scattering solutions for plane, cylindrical, and spherical apertures, *IEEE Trans. on Biomed. Eng.*, **28** (1981) 200–202.

- [28] L. Nguyen, A family of inversion formulas in thermoacoustic tomography, *Inverse Problems and Imaging*, **3** (2009) 649–675.
- [29] A. A. Oraevsky, S. L. Jacques, R. O. Esenaliev, and F. K. Tittel, Laser-based photoacoustic imaging in biological tissues, *Proc. SPIE*, **2134A** (1994) 122–8.
- [30] B. J. Roth and K. Schalte, Ultrasonically-induced Lorentz force tomography, *Med. Biol. Eng. Comput.* **47** (2009) 573–7.
- [31] A. M. Stewart, Longitudinal and transverse components of a vector field, *Classical Physics*. In press, <http://arxiv.org/abs/0801.0335v2>.
- [32] V. S. Vladimirov, *Equations of mathematical physics*. (Translated from the Russian by Audrey Littlewood. Edited by Alan Jeffrey.) Pure and Applied Mathematics, **3** Marcel Dekker, New York (1971).
- [33] Wang L V (Editor) 2009 "*Photoacoustic imaging and spectroscopy*" (CRC Press).
- [34] H. Wen, J. Shah, R. S. Balaban, Hall effect imaging, *IEEE Trans. Biomed. Eng.*, **45** (1998) 119–24.
- [35] M. Xu and L.-H. V. Wang, Time-domain reconstruction for thermoacoustic tomography in a spherical geometry, *IEEE Trans. Med. Imag.*, **21** (2002) 814–822.
- [36] H. Zhang and L. Wang, Acousto-electric tomography, *Proc. SPIE* **5320** (2004) 145–9.